




# The Extract of *Ilex cornuta* Bark Promotes Bone Healing by Activating Adenosine A2A Receptor

Xi Zheng <sup>1</sup>, Jingyi Wang<sup>1</sup>, Junlin Zhou <sup>2</sup>, Dong Wang <sup>2</sup>

<sup>1</sup>Department of SICU, Beijing Chaoyang Hospital, Capital Medical University, Beijing, 100020, People's Republic of China; <sup>2</sup>Department of Orthopedics, Beijing Chaoyang Hospital, Capital Medical University, Beijing, 100020, People's Republic of China

Correspondence: Dong Wang, Department of Orthopedics, Beijing Chaoyang hospital, Capital Medical University, 8 Gongren Tiyuchang Nanlu, Chaoyang District, Beijing, 100020, People's Republic of China, Tel +86-13240718193, Email dongwang\_article@outlook.com

**Introduction:** Bone fracture is a common reason causing human disability. The delay union and nonunion rates are approximately 5–10% despite patients receiving active treatment. Currently, there is a limited number of drugs directly accelerating bone healing, especially direct extracts from plants. Moreover, the pharmacological effects of *Ilex cornuta* bark are still unknown. This study aimed to explore the effects and mechanisms of *Ilex cornuta* bark in bone healing.

**Methods and Results:** First, the promoting effects of *Ilex cornuta* bark on bone healing were verified by the mice femur fracture model as *Ilex cornuta* bark increased the callus formation and enhanced the biomechanical stability during the bone healing process. Second, the target gene of *Ilex cornuta* bark in bone healing identified by bioinformatics analysis and immunofluorescence validation was *ADORA2A*. Third, 410 main compound compositions of *Ilex cornuta* bark were explored by a non-target metabolomic analysis, where 190 of them were neg ion mode, and 220 were pos ion mode. Molecular docking was used to predict the regulatory effect of the compounds on adora2a (adenosine A2A receptor), and ursonic acid had the lowest binding energy with adora2a. Finally, *nfkbl* was the transcription factor (TF) of adora2a, and ursonic acid also had the lowest binding energy by bioinformatic analysis and molecular docking.

**Conclusion:** Overall, *Ilex cornuta* bark water extract was a new plant extract on promoting bone healing; in addition, the mechanism of it might be activating adora2a though *Nfkbl*.

**Keywords:** *Ilex cornuta* bark, adenosine A2A receptor, bone healing, non-target metabolomic analysis, bioinformatic analysis, *Nfkbl*

## Plain Language Summary

In the present study, we discussed the effect of a new plant extract on promoting bone healing and explored its mechanism. The bone delay union and nonunion rates are approximately 5–10% despite patients receiving active treatment. Currently, there are still few plant extracts directly promoting fracture healing, and many plant extracts need to be developed.

## Introduction

Research on and development of new drugs to promote bone healing has always been a hotspot because the bone delay union and nonunion rates are approximately 5–10% despite patients receiving active treatment.<sup>1–4</sup> Currently, there are still few plant extracts directly promoting fracture healing, and many plant extracts need to be developed.

Zura et al<sup>1</sup> summarized the impact factors of delayed bone union and nonunion and proposed that multiple concurrent fractures, prescription nonsteroidal anti-inflammatory drug and opioid use, open fracture, anticoagulant use, and osteoarthritis with rheumatoid arthritis were the most important factors. At present, there are many therapeutic drugs for fracture healing, but there are uncertainties and adverse reactions, such as malignant tumors, secondary fractures, liver and kidney injury, urinary stones.<sup>2,3</sup> Plants are being considered as an alternative therapy to promote fracture healing.

*Ilex cornuta* (Aquifoliaceae) is an evergreen shrub widely distributed in China and Korea. Its leaves are one of the major formulas of “Ku-Ding-Cha”, which is a popular tonic tea used for sore throat, obesity, cardiovascular disease, arthrodynia, acute conjunctivitis, headache, toothache, rheumatic arthralgia, and urticaria.<sup>5,6</sup> Currently, studies have been

focusing on *Ilex cornuta* leaves, roots, or their extracts in cardiovascular and inflammatory diseases. However, the pharmacological effects of the bark remain unknown.

Adenosine A2A receptor (adora2a) is a member of the G-protein coupled receptor family and has immune and inflammatory response regulation effects.<sup>3,7,8</sup> Recently, some studies have proposed that adora2a agonist was similar to bone morphogenetic protein-2 (BMP-2) in promoting fracture healing.<sup>7</sup> The mechanism of adora2a in bone healing might be related to the Wnt/ $\beta$ -catenin and activating protein-1 pathways.<sup>9,10</sup> Presently, there has been no plant extract to promote fracture healing by activating adora2a.

This study aimed to explore the effects and mechanisms of *Ilex cornuta* bark in bone healing. First, the mice femur fracture model was used to verify the promoting role of *Ilex cornuta* bark in bone healing by microcomputed tomography and finite element analysis. Second, the target genes and related regulatory mechanisms of *Ilex cornuta* bark were expounded by bioinformatic analysis. Third, the compound composition of *Ilex cornuta* bark was revealed by non-target metabolomic analysis. Finally, molecular docking and immunofluorescence were used to verify the target genes.

## Materials and Methods

### Preparation of *Ilex cornuta* Bark

The bark of *Ilex cornuta* was purchased from Ningbo Lanzhuang, Zhejiang Province, China. The water extract of the bark was prepared according to the following procedure: 500 g of bark was dried in the shade and ground into crude powder. Then, the crude powder was immersed in water (v/w, 10:1) for 1 h, followed by its heating at 100°C for 2 h. The extraction solution was filtered by 35 mesh sieves, and the filtrate (the water extract of the bark) was kept at -20°C until use (Figure 1).

### Animals

Female adult BALB/c mice (Vital River Laboratories, Laboratory Animal Institution Accreditation Certificate Registration Number: CNAS LA0004, 18–20 g) were kept in separate sterile cages and had free access to a sterilized chow diet and water. The feeding environment was specific-pathogen-free under a 12-h light/dark cycle at 23.6°C and 35% humidity. Animal welfare and experimental procedures complied with the principles of Laboratory Animal Guidelines for Ethical Review of Animal Welfare (GB/T 35892–2018). The present study was approved by the Capital Medical University ethics committee on the use of animals in research and education (approval no. AEEI-2021-308). The following humane endpoints were applied: extreme difficulty in moving to get food or water; severe wound infection; limb necrosis; auto-mutilation; and screaming in response to a gentle touch.

At the end of the experiments or when the humane endpoints were reached, the mice were euthanized via an excessive dose of sodium pentobarbital (100 mg/kg, intraperitoneal injection). The ethical code of animal experiments is AEEI-2021-308. Animal death was confirmed by the absence of breathing or heartbeat.

### Animal Sample Size

The required animal sample size was calculated by Stata/SE 12.0 (StataCorp LP, USA) software. There have been no studies on *Ilex cornuta* or its extract regarding bone healing so far; hence, the sample size was estimated by referring to previous studies on the promotion of fracture healing by adora2a agonists.<sup>3</sup> The promotion rate of adora2a agonists was 100%, and the promotion rate of control group was 0% at 8 weeks of bone healing in the study. Besides,  $\alpha$  was set as 0.05 (two-sided), the model failure rate was about 10%, and  $1-\beta$  was set as 0.80. Therefore, at least 5 mice were needed for each time point (7, 14, and 21 days) in each group.

### Femur Fracture Model

The fracture model used was similar to previous literature reports.<sup>11–13</sup> Briefly, mice were anesthetized with 3% isoflurane and 800 mL/min oxygen. After successful anesthesia, the mice were placed in the left lateral position on the small animal operating table. The right thigh was shaved, disinfected with 75% ethanol 3 times, and wrapped with a sterile hole towel. The posterolateral incision of the right thigh with a length of 5 mm was made. The skin and subcutaneous tissue were cut, and a deep fascia was bluntly separated. The femoral shaft was exposed through the space

between tensor fascia lata and lateral femoral muscle. A transverse fracture of the middle femur was made by scissors and stabilized with the retrograde placement of a 25G syringe needle (0.5 mm × 20 mm, KLmedical, China). The incision was closed by using a 5–0 absorbable band (Ethicon, USA). To prevent infection, mice received 200 ug gentamicin intramuscular injection daily for three days after being modeled.

## Animal Grouping and Sample Harvest

Thirty mice with femur fracture were divided into 2 groups: the *Ilex cornuta* group (n = 15) and the control group (n = 15). Mice in the *Ilex cornuta* group were given 0.5 mL water extract of the *Ilex cornuta* bark intragastrically once a day after being fracture modeled until the observation endpoint. Mice in the control group were treated daily with 0.5 mL of the physiological saline intragastrically until the observation endpoint (Figure 1).

Mice were sacrificed at 7, 14, and 21 days after being fracture modeled by pentobarbital intraperitoneal injection. The right femur samples were harvested and stored immediately with AllProtect™ stabilization reagent (R0121-100 mL, Beyotime, China) at –80°C for further analysis.

## Microcomputed Tomography (μCT)

Samples were scanned by using Bruker Micro-CT Skyscan 1276 system (Kontich, Belgium) which was finished in Wuhan Duobo Technology Co., Ltd. The 25G syringe needle was taken out before the μCT examination. Scan settings were as follows: voxel size of 6.5 μm, medium resolution, 85 kV, 200 mA, 1-mm Al filter, and integration time of 384 ms. Density measurements were calibrated to the manufacturer's calcium hydroxyapatite (CaHA) phantom. Two-dimensional reconstruction was accomplished by NRecon (version 1.7.4.2). Sequential images were obtained at slice distances of 6.5 μm. The pixel size of the obtained image was 1400 × 1400. Mimics research 21.00 was used for three-dimensional reconstruction. The Hounsfield unit thresholding of bone was >100 GV, and that of callus was 80–99 GV. The bone volume (BV), callus volume (CV), BV/total volume (TV, TV = BV + CV), and CV/

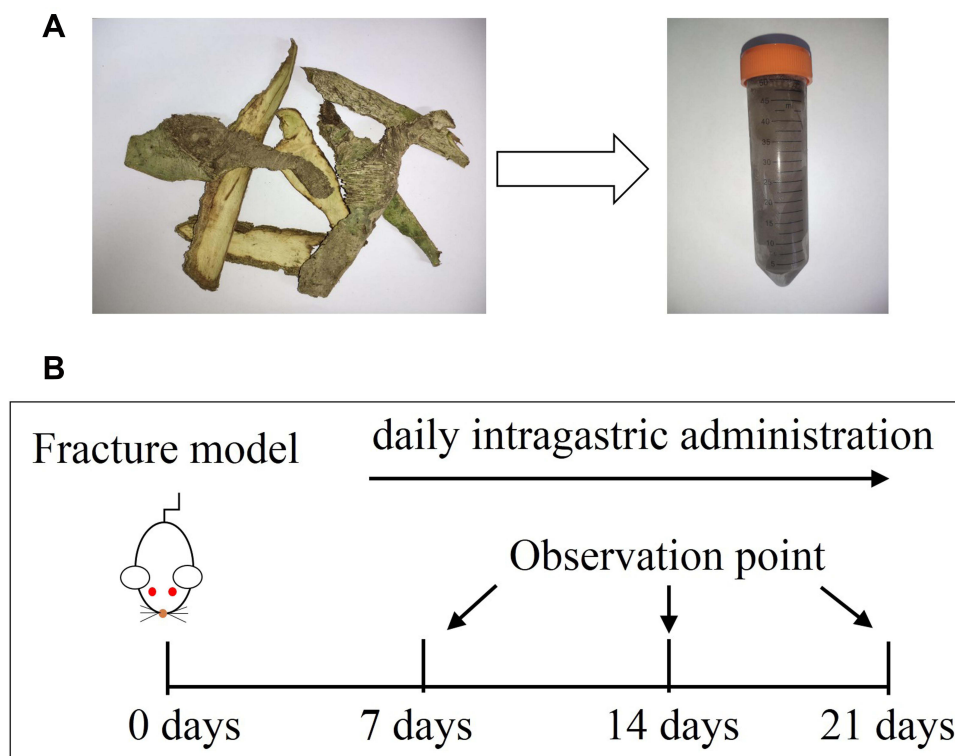


**Figure 1** The *Ilex cornuta* bark and a schematic diagram. (A) The *Ilex cornuta* bark and its water extracts. (B) The animal experiments design. 30 mice with femur fracture were received daily intragastric administration treatment. The observation time points were 7,14,21 days.

TV of the region of interest (ROI) (200 axial slices above and below the fracture line) were calculated by Mimics research software.

## Finite Element Analysis

The biomechanical strength of bone was evaluated by a finite element analysis. After the three-dimensional reconstruction of  $\mu$ CT data was accomplished by Mimics research 21.00, the three-dimensional structure was divided into hexahedral volume meshes with  $0.13 \times 0.13 \times 0.13 \text{ mm}^3$  mesh size. The material property assignment of the meshes was based on the  $\mu$ CT image gray value. The conversion formulae between gray value and material property value were as follows: material density =  $-13.4 + 1017 \times (\mu\text{CT gray value})$ ; Young's modulus =  $-388.8 + 5925 \times (\text{material density})$ ; and Poisson's ratio = 0.3.<sup>14,15</sup> Then, the cdb format file was exported and imported into ANSYS workbench 17.0. The axial stress and rotational stress of the femur were evaluated.

## Non-Target Metabolomics Analysis

The non-target metabolomic analysis was accomplished in Beijing Qinyi Biotechnology Co., Ltd. The crude powder of the bark of *Ilex cornuta* was comminuted ultrasonically (45 Hz, 30s). Then, 100 mg comminuted bark was added to 500  $\mu\text{L}$  of the extraction solution (the methanol: water ratio was 4:1), followed by homogenization at 45 Hz for 4 min and sonication for 1 h in an ice-water bath. Afterward, the bark sample was centrifuged at 12,000 rpm for 15 min at 4°C and placed for 1 h under  $-40^\circ\text{C}$ .

The supernatant was filtered by a 0.22- $\mu\text{m}$  filter and stored at  $-80^\circ\text{C}$  for an LC-MS/MS analysis.

Agilent 1290 infinity liquid chromatograph (Agilent, USA) coupled with Q Exactive Focus mass spectrometry (Thermo Fisher Scientific, USA) was used to perform the LC-MS/MS analysis. UPLC BEH C18 column ( $1.7 \mu\text{m} \times 2.1 \text{ mm} \times 100 \text{ mm}$ , Waters, USA) was used to separate the compounds of the filtrate. The mobile phase consisted of 0.1% formic acid in water (A) and 0.1% formic acid in acetonitrile (B). The flow rate was set at 0.4 mL/min, and the sample injection volume was set at 5  $\mu\text{L}$ . The multi-step linear elution gradient program was as follows: 0–3.5 min, 95–85% A; 3.5–6 min, 85–70% A; 6–6.5 min, 70–70% A; 6.5–12 min, 70–30% A; 12–12.5 min, 30–30% A; 12.5–18 min, 30–0% A; 18–25 min, 0–0% A; 25–26 min, 0–95% A; 26–30 min, 95–95% A.

Q Exactive Focus mass spectrometer, and Xcalibur software (Thermo Fisher Scientific, USA) were used to obtain the MS and MS/MS data based on the information-dependent acquisition (IDA) mode. The parameters were set as follows: a sheath gas flow rate of 45 Arb, aux gas flow rate of 15 Arb, capillary temperature of  $400^\circ\text{C}$ , full MS resolution of 70,000, MS/MS resolution of 17,500, collision energy of 15/30/45 in NCE mode, and spray voltage of 4.0 kV (positive) or  $-3.6 \text{ kV}$  (negative).

The identification and structural analyses of the primary and secondary spectral data of the metabolites detected by mass spectrometry were based on the BIOTREE TCM database of Shanghai BIOTREE Biological Technology Co., Ltd. (Shanghai, China).

## Bioinformatics Analysis of Target Genes and Molecular Docking

The HERB database (herb.ac.cn) was used to predict the target genes of *Ilex cornuta*.<sup>16</sup> HERB is an open and free-access database containing 7263 herbs, 12,933 target genes, and 1966 references. The target genes are partially obtained from the manual curation from PubMed references, and others are obtained from previous databases, including SymMap, HIT, TCMSP, and TCMi. The STRING database (cn.string-db.org, version 11.5) was used to construct the protein–protein interaction (PPI) network of the target genes.<sup>17,18</sup> The confidence score was set as  $\geq 0.4$ . Cytoscape 3.8.2 ([www.cytoscape.org](http://www.cytoscape.org)) software and cytoNCA app were used to analyze the PPI network and make the result visualization.<sup>19–21</sup> The TRRUST database ([www.gmpedia.org/trrust](http://www.gmpedia.org/trrust), version 2.0) was used to predict the transcription factors (TFs) of the target genes.<sup>22</sup> TRRUST is a database containing 8444 and 6552 TFs–target regulatory relationships of 800 human TFs and 828 mouse TFs, respectively. JASPAR 2022 ([jaspar.genereg.net](http://jaspar.genereg.net)) was used to predict the binding region of TFs and *ADORA2A* promoter sequence.<sup>23</sup> DAVID Bioinformatics Resources 6.8 ([david.ncifcrf.gov](http://david.ncifcrf.gov)) was used to make gene ontology (GO) annotations and Kyoto encyclopedia of genes and genomes (KEGG) pathways for the target genes.<sup>24,25</sup> The criterion was gene counts  $>2$ .

The molecular docking method was as follows. Briefly, the target genes and their TFs represented receptors, while the main ingredients of *Ilex cornuta* represented the ligands. The molecular structure of the genes or TFs was obtained from the PDB database ([www.rcsb.org](http://www.rcsb.org)). Additionally, the structure of the main ingredients was acquired from the ChemSpider database ([www.chemspider.com](http://www.chemspider.com)).<sup>26–28</sup> PyMOL software ([pymol.org/2](http://pymol.org/2)) was used to remove the water molecules and ligand structures in genes or TFs structures obtained from the PDB database.<sup>29</sup> AutoDock 4.2 software ([autodock.scripps.edu/downloads](http://autodock.scripps.edu/downloads)) was used for molecular docking and analyzing the binding energy. PyMOL software was used to display the binding hydrogen bond and binding site between the receptor and the ligand.

## Immunofluorescence Verification

The right femur samples were fixed with 4% paraformaldehyde for 24 h and decalcified in 20% EDTA solution for 6 weeks. Then, the samples were dehydrated by gradient concentration ethanol, followed by clearing in xylene and embedding in paraffin. Afterward, the tissue samples were sectioned at 4  $\mu\text{m}$  thickness for further study.

Immunofluorescence was as follows. Briefly, the tissue section was dewaxed with xylene and ethanol. Then, the section was repaired by EDTA antigen repair buffer (PH8.0) (Servicebio, China) and blocked with 3% BSA (Servicebio, China) for 30 min, followed by incubation with the relevant primary rabbit antibody (1:200, Affinity, China) overnight at 4°C. Then, the sections were washed by PBS 3 times and incubated with FITC-conjugated donkey anti-rabbit IgG (H + L) (1:100, Servicebio, China) at room temperature in the dark for 50 min. Afterward, the sections were washed by PBS 3 times and stained with DAPI in the dark for 10 min, followed by washing by PBS 3 times again and incubating with tissue autofluorescence quenching agent I in the dark for 10 min. Then, the sections were sealed by an anti-fluorescence quenching sealing agent (Servicebio, China). The fluorescence was observed with an inverted fluorescence microscope, and all the images were analyzed by Image-pro plus 6.0 (details of the analysis methods are presented in [Supplementary Material 1 Figures 1–5](#)).

## Statistical Analysis

The normality of the data was analyzed by Shapiro–Wilk test. The measurement data were described as mean  $\pm$  standard deviation and compared via independent-sample *t*-test between the two groups or one-way ANOVA between more than the two groups if data were normally distributed. Additionally, the least significant difference (LSD) tests were used for post hoc analysis. Otherwise, the measurement data were described as the median (interquartile range) and compared by Mann–Whitney *U*-test between the two groups or Kruskal–Wallis H-test between more than the two groups. Mann–Whitney *U*-test was also used as a post hoc test following Kruskal–Wallis H-test. The enumeration data were represented by occurrence rate and compared by Chi-square test or Fisher's exact test.  $P < 0.05$  was considered statistically significant.

## Results

### The Extract of the *Ilex cornuta* Bark Accelerated Callus Formation in Mice Femur Fracture Model

Mice underwent right femur shaft transverse fracture and were divided into 2 groups. Mice in the *Ilex cornuta* group were treated with the water extract of *Ilex cornuta* bark and had more callus in the coronal, sagittal, and axial views on days 14 and 21 ([Figure 2](#)).

The fractured femur was reconstructed based on the CT scan images after the 25G syringe needle was taken out. The Hounsfield unit thresholding of bone was  $>100$  GV, and the callus was 80–99 GV. Bone tissue and callus were colored in purple and yellow, respectively. The three-dimensional reconstruction images of the full-length femur displayed that the mice in the *Ilex cornuta* group had more mineralized tissue (bone tissue) in the fracture site than the control group ([Figure 3A](#)). The 200 axial slices above and below the fracture line were set as ROI. The three-dimensional reconstruction images of the fracture site showed that the *Ilex cornuta* group had more callus tissue in the fracture site ([Figure 3A](#)). Meanwhile, the bar chart revealed that there was a significant difference between the two groups in CV, BV/TV, and CV/TV on days 14 and 21 in the fracture site ( $p < 0.05$ ) ([Figure 3B](#)).

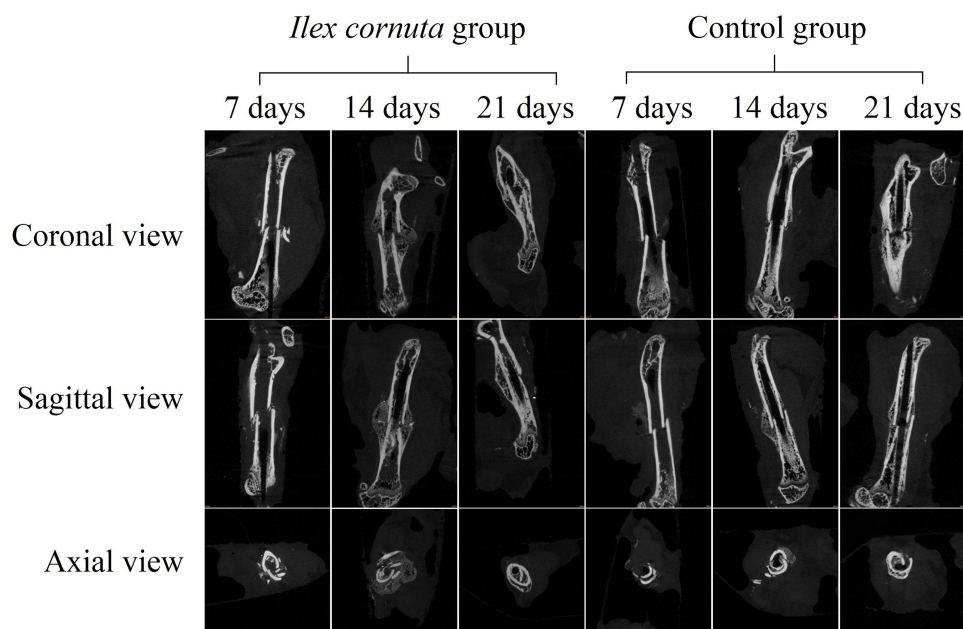


**Figure 2** The different views of  $\mu$ CT in 7, 14 days and 21 days. The images showed that mice received *Ilex cornuta* bark treatment had more callus in the coronal view, sagittal view, axial view in 14 days and 21 days.

## The Plant Extract Enhanced the Biomechanical Strength of the Bone Healing Process

The finite element analysis was used to evaluate the biomechanical strength of the fractured femur. One N force was applied to the upper part of the femur, and the distal femur was fixed. The femur of the mice in the *Ilex cornuta* group exhibited lower axial stress and strain than that of the control group, and the differences were statistically significant at 21 days ( $p < 0.05$ ) (Figure 4). Therefore, the mice of the *Ilex cornuta* group had stronger axial mechanical stability.

0.5 N  $\times$  m torsion force was exerted on the upper part of the femur, and the distal femur was fixed. Additionally, the result was similar to that of axial biomechanical strength. The mice of the *Ilex cornuta* group had lower torsional stress and strain at 21 days ( $p < 0.05$ ), meaning that the *Ilex cornuta* group had stronger torsional mechanical stability (Figure 4).

## ADORA2A Was the Key Target Gene of the *Ilex cornuta* Bark in Promoting Bone Healing

The HERB database and the STRING database were used to predict the target genes of *Ilex cornuta* bark in accelerating fracture healing. A total of 206 target genes were involved, and *ADORA2A* was one of the most significantly different genes. Additionally, the  $-\log_{10}$ FDR of *ADORA2A* was 4.85389, and  $\log_2$ (P-value) was 23.10115 (Figure 5A) (details of the target genes are presented in Supplementary Material 2). The target genes were constructed using a protein–protein interaction (PPI) network by the STRING database. The network stats were as follows: the number of nodes was 195, the number of edges was 1056, the average node degree was 10.8, the average local clustering coefficient was 0.533, the expected number of edges was 444, and the PPI enrichment p-value was  $< 1.0e-16$  (Figure 5B; 206 target genes are colored in purple).

Cytoscape software and cytoNCA app were used to analyze the PPI network, and the results of different algorithms on *ADORA2A* in the PPI network were as follows: the betweenness value was 1002.58, the degree value was 20, and the closeness value was 0.23 (Figure 5B; a circular gene analysis image showed the betweenness value rank of *ADORA2A*, where the purple represents a high value and yellow represents a low value).

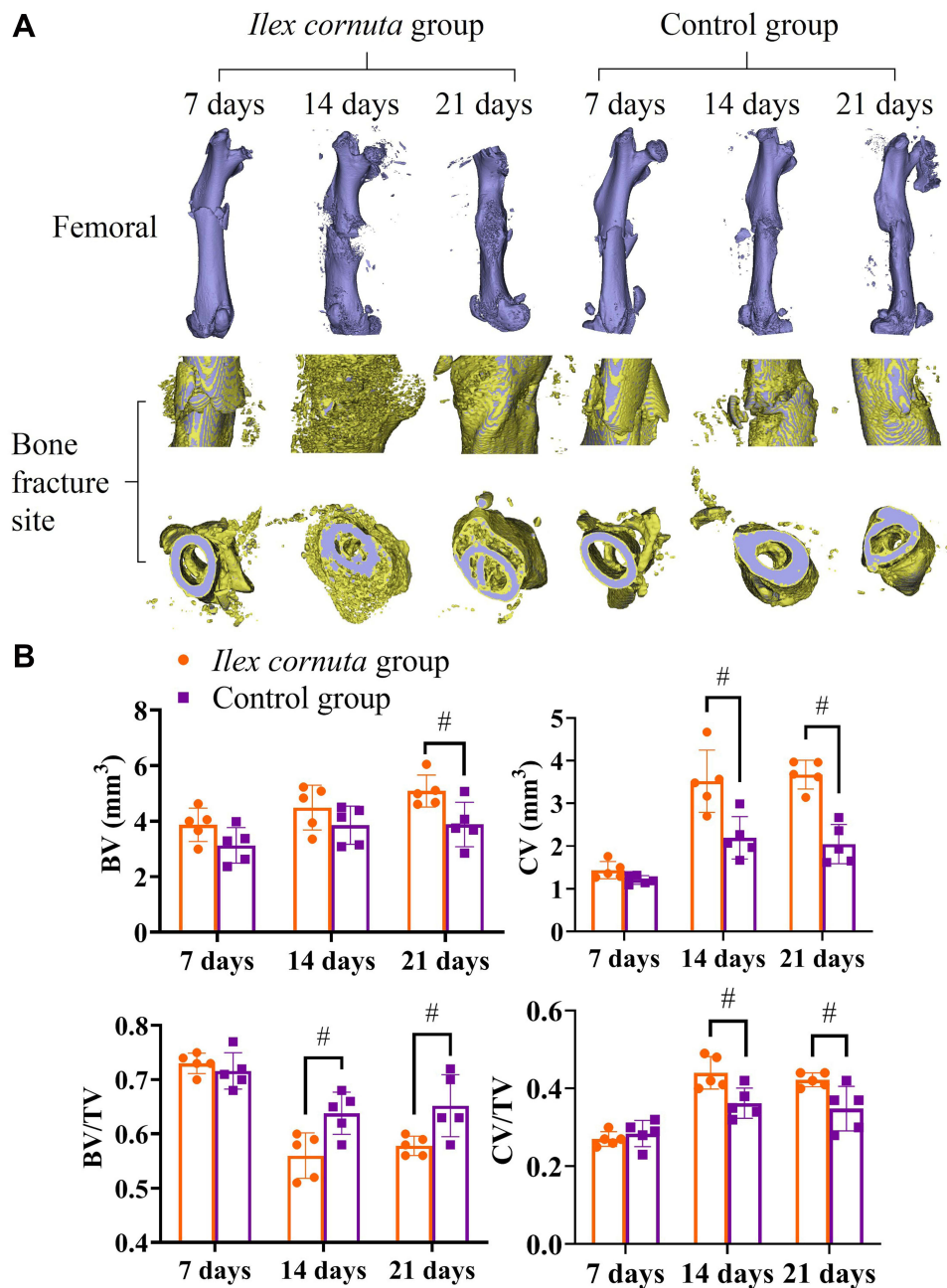
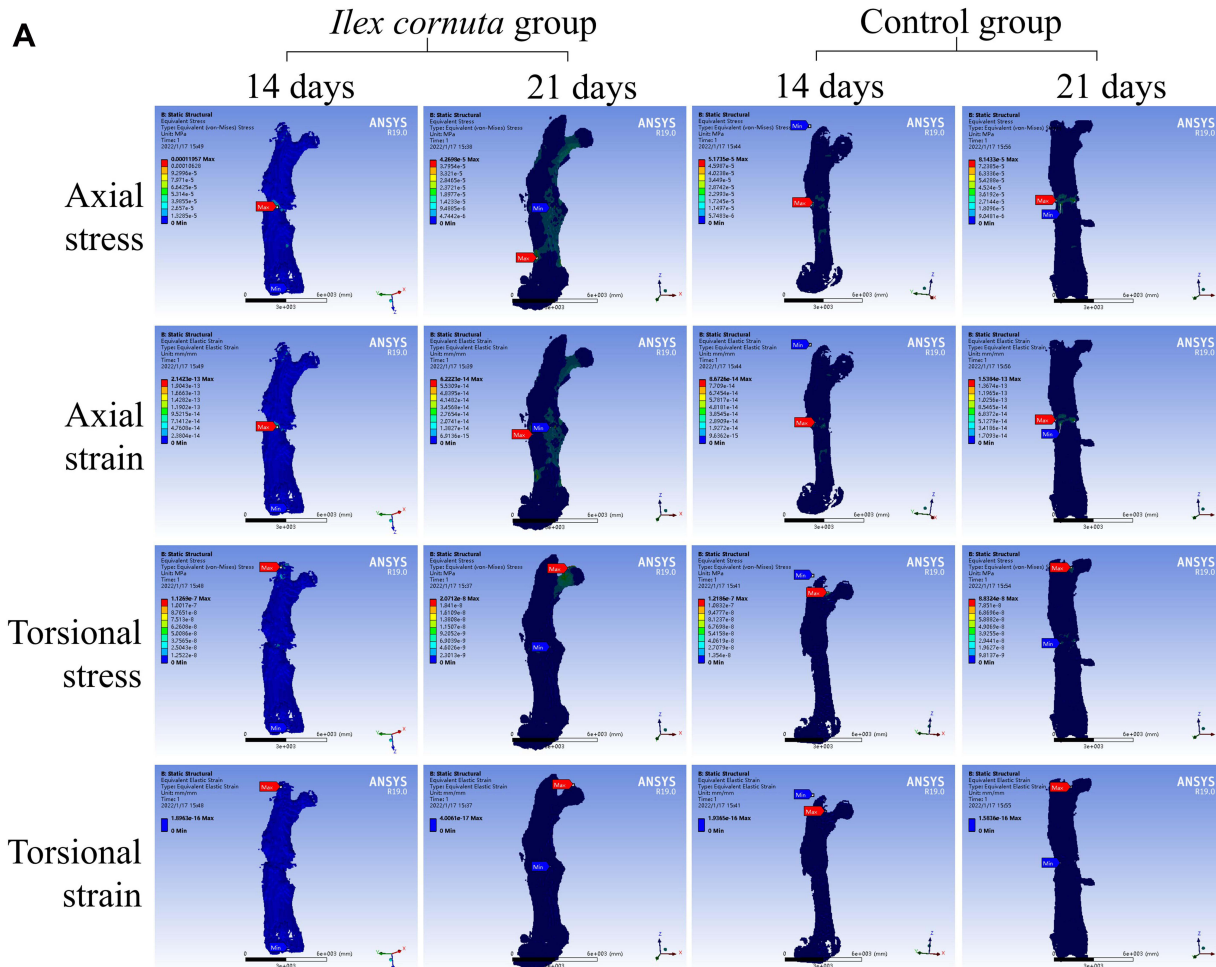


**Figure 3** *Ilex cornuta* bark on callus formation in 7, 14 days and 21 days. (A) the three-dimensional reconstruction images of femur and fracture site. Bone tissue was colored as purple and callus was yellow. *Ilex cornuta* group mice had more callus and mineralized tissue in fracture site at 14,21 days. (B) The bar chart revealed the difference between groups, #  $p < 0.05$ .  $n = 5$  at each timepoint.

## cAMP Signaling Pathway and Neuroactive Ligand–Receptor Interaction Might Be the Most Important Pathways of the *Ilex cornuta* Bark in Promoting Bone Healing

Cytoscape software was used to select *ADORA2A* and related regulatory genes of *adora2a* among 207 target genes of the *Ilex cornuta* bark in promoting bone healing (Figure 5B). DAVID database was used to analyze the involved pathways of *ADORA2A* and related regulatory genes of *adora2a* (Figure 6). Thirty-two pathways were enriched, and 7 genes were enriched in a cAMP signaling pathway, such as *CREB1*, *ADORA2A*, *FSHB*, *ADORA1*, *GNAS*, *FOS*, and *DRD2* (Figure 7A). Besides, the p-value of the cAMP signaling pathway was 3.76e-06. Meanwhile, neuroactive ligand-receptor interaction also had 7 genes enriched, and the p-value was 3.13e-05. The cAMP signaling pathway and



- B**
- *Ilex cornuta* group
  - Control group

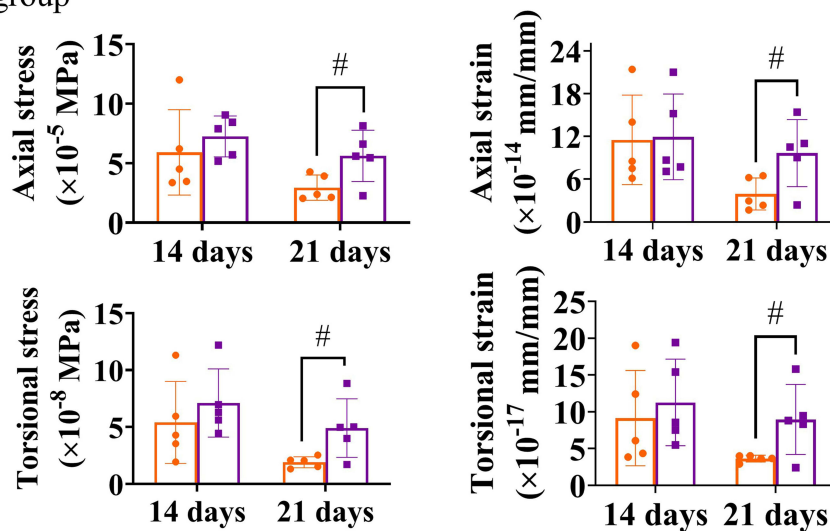


**Figure 4** *Ilex cornuta* bark on biomechanical strength of bone healing process. **(A)** The equivalent stress and strain maps. Mice received *Ilex cornuta* bark treatment had less stress and strain at 21 days. **(B)** The bar chart revealed the difference between groups, #  $p < 0.05$ ,  $n = 5$  at each timepoint.



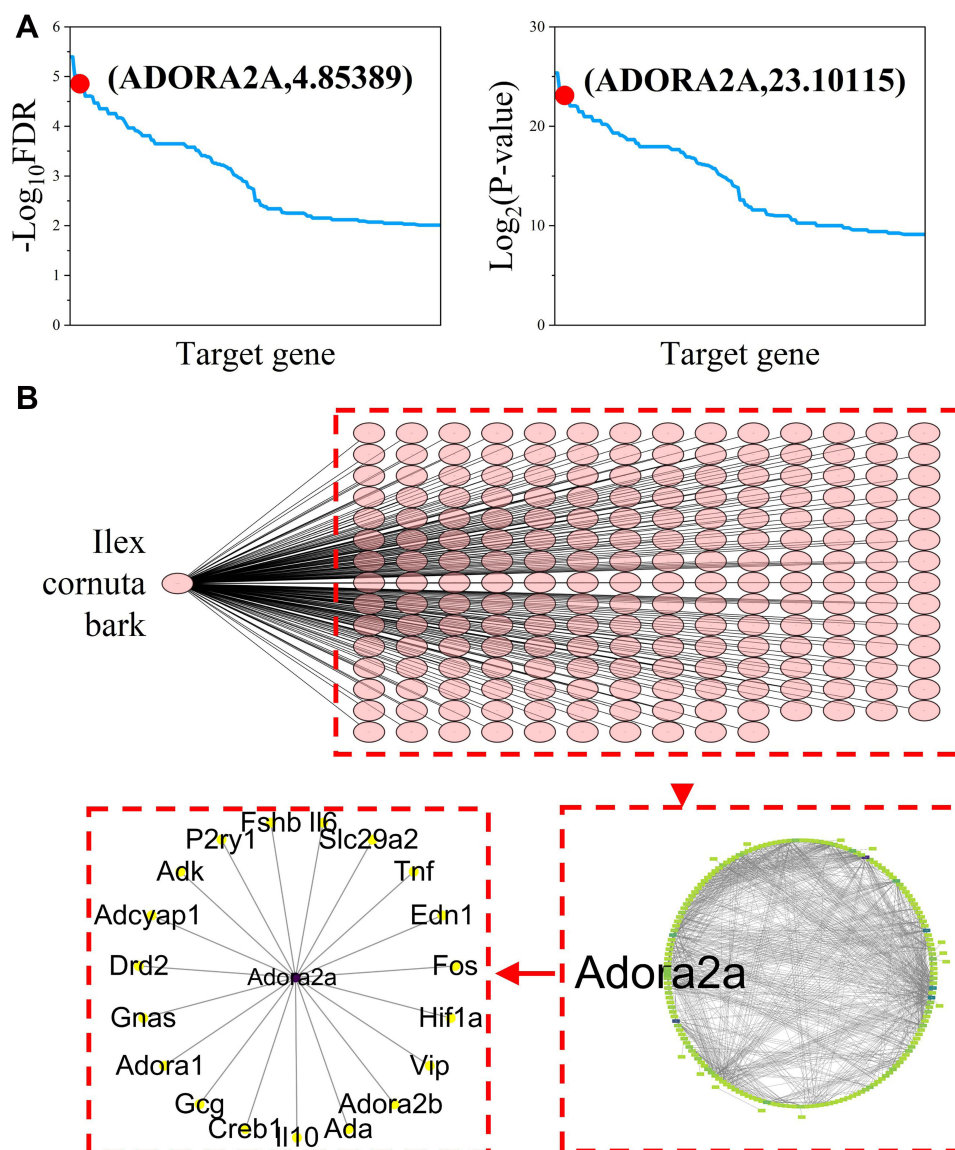


**Figure 5** The target genes of *Ilex cornuta* bark on bone healing by bioinformatics analysis. **(A)** The line chart of  $-\log_{10}FDR$  and  $\log_2(P\text{-value})$  value of the 206 target genes. **(B)** The PPI networks of *Ilex cornuta* bark target genes. The target 206 genes were ranked by betweenness value as yellow to dark purple. *Adora2a* was the key gene of the PPI network and had 19 target genes.

neuroactive ligand–receptor interaction were the main pathways of *ADORA2A* and related regulatory genes enriched (Figure 7A). Considering the important role of *ADORA2A* and related regulatory genes of the *Ilex cornuta* bark in promoting bone healing, the cAMP signaling pathway and neuroactive ligand–receptor interaction might be the most important pathways of the *Ilex cornuta* bark in accelerating bone healing.

### The *Ilex cornuta* Bark Had 410 Main Compound Compositions, and Ursonic Acid Might Be the Main Compound That Activated *ADORA2A*

Non-target metabolomic analysis was used to explore the main compositions of the *Ilex cornuta* bark. The *Ilex cornuta* bark had 410 compounds, of which 190 were neg ion mode, and 220 were pos ion mode (Figure 7B and C; Table 1) (details of the main compound compositions are presented in Supplementary Material 3). The top 10 compounds of content were picked, and molecular docking methods were used to predict the binding possibility of the compound and

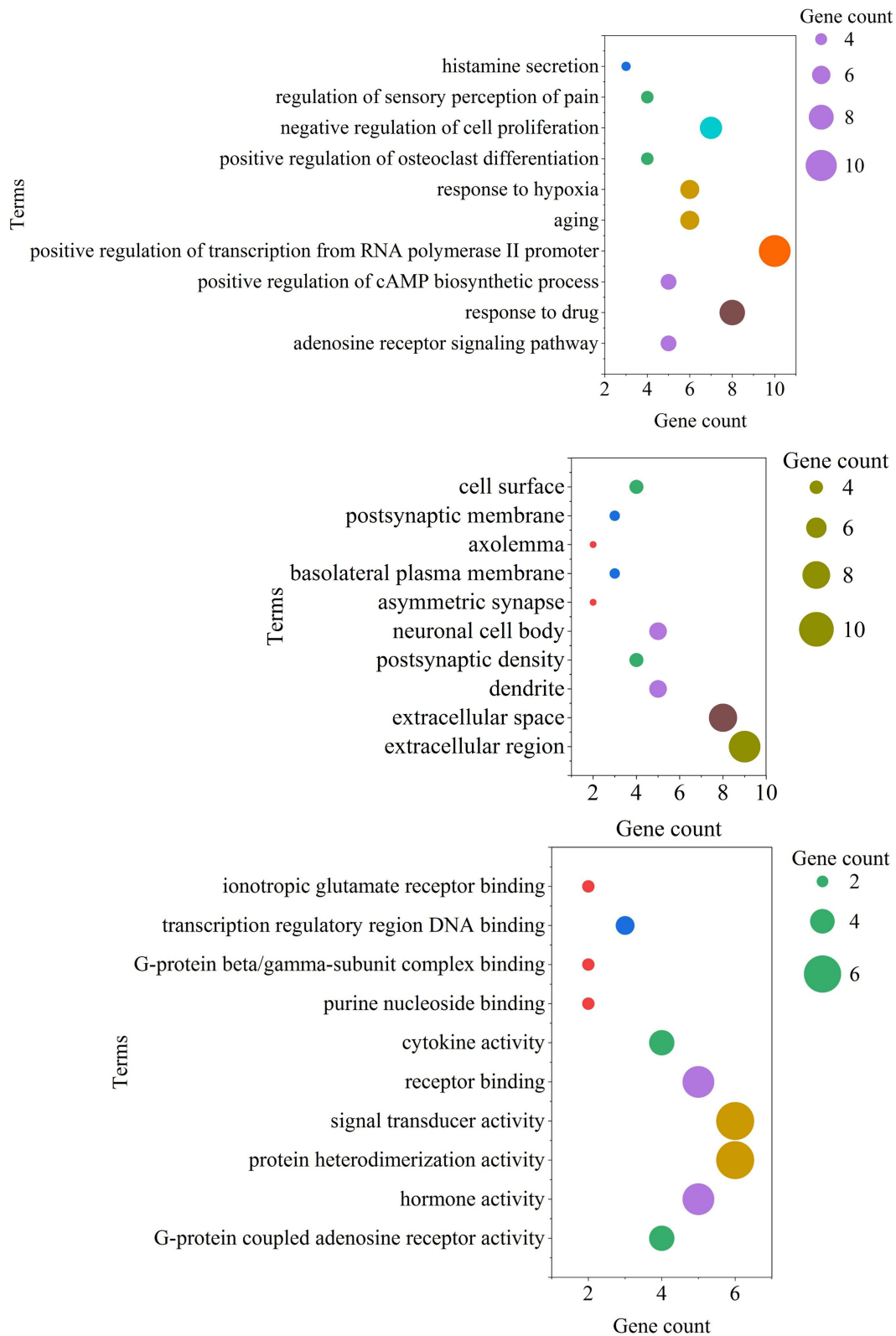


**Figure 6** The GO enrichment results of adora2a and related target genes. The scatter diagram showed the top 10 enriched terms of biological process, cellular component and molecular function.

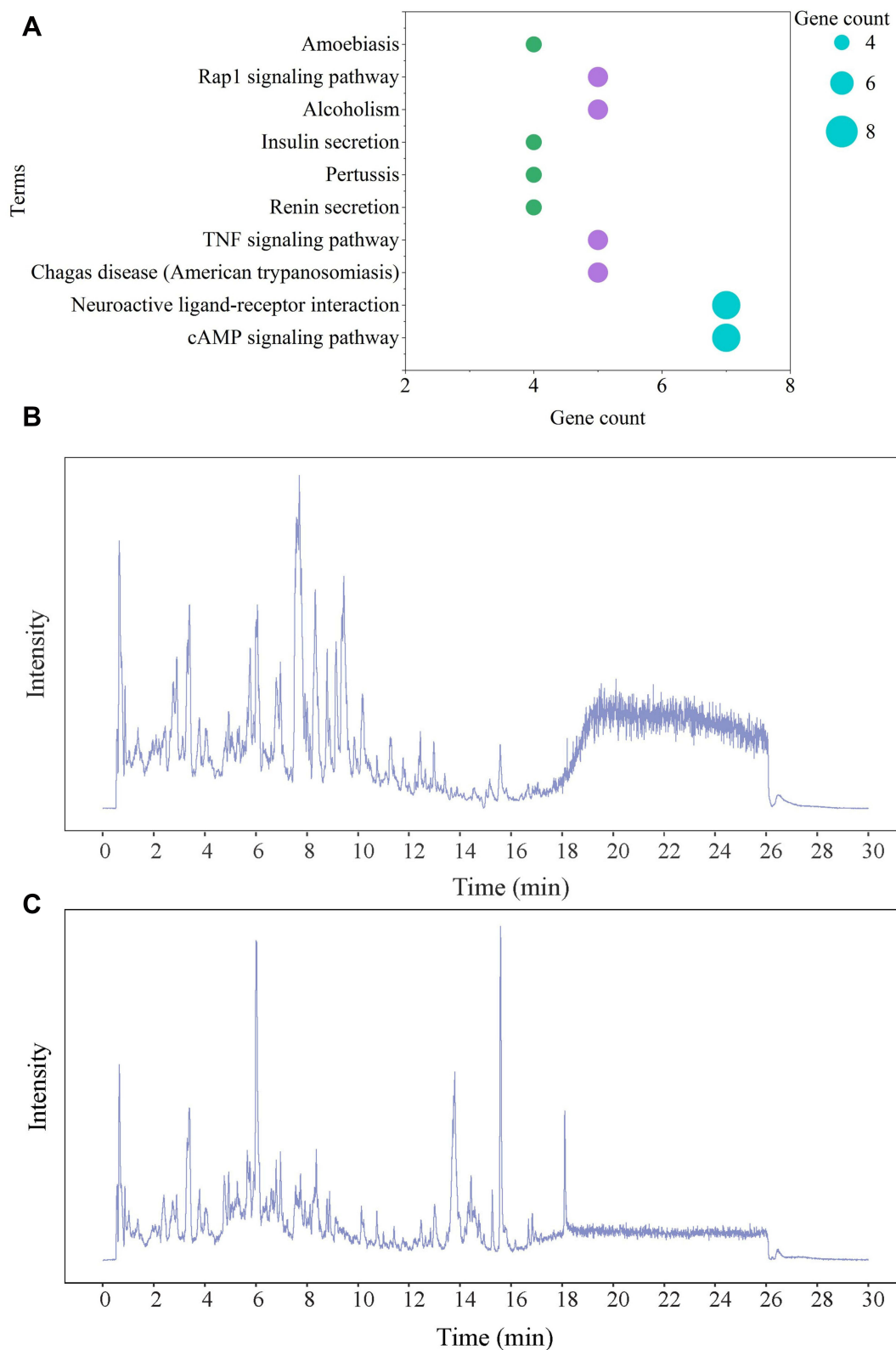


**Figure 7** The KEGG enrichment and non-target metabolomics analysis results. **(A)** The scatter diagram showed the top 10 enriched pathways. cAMP signaling pathway and neuroactive ligand–receptor interaction had the most involved genes. **(B)** The images showed the main negative modes compound compositions of *Ilex cornuta* bark. **(C)** The images showed the main positive modes compound compositions of *Ilex cornuta* bark.

**Table I** The Top 20 Main Compound Compositions of *Ilex cornuta* Bark

Compound Name	Composite Score	Content (%)	InChIKey	SMILES	Formula	m/z	Retention Time(s)	Ion Mode
Erucamide	0.816621	0.10956	UAUDZVJPLUQNMU-KTKRTIGZSA-N	<chem>NC(=O)CCCCCCCCCCC/C=C\CCCCCCCC</chem>	C22H43NO	338.3416	1086.58	Pos
Chlorogenic acid	0.847098	0.088001	CWVVRJTMFETXNAD-JUHZACGLSA-N	<chem>C1C(C(C(C(C1(=O)O)O)OC(=O)C=CC2=CC(=C(C=C2)O)O)O)O</chem>	C16H18O9	353.0874	169.773	Neg
Ursonic acid	0.956054	0.033714	MUCRYNWJQNHDJH-OADIDDRXSA-N	<chem>CC1CCC2(CCC3(C(=CCC4C3(CCC5C4(CCC(=O)C5(C)C)C)C2C1C)C)C(=O)O</chem>	C30H46O3	455.3522	458.103	Pos
1a,5,7a-Trimethyl-2,2a,6,6a,7a,8,9,9a-octahydrobisoxireno [4,5:8,9]cyclodeca[1,2-b]furan-4(1aH)-one	0.893502	0.031829	CWAJEURPJYKGRU-UHFFFAOYSA-N	<chem>CC1=C2/CC3OC3(C)CCC4OC4(C)CC2OC1=O</chem>	C15H20O4	265.1434	163.26	Pos
Methylxanthoxylin	0.64304	0.031759	AAOFJKLTKOQTQ-UHFFFAOYSA-N	<chem>O=C(C(=1C(O)=C(C(OC)=CC1OC)C)C</chem>	C11H14O4	211.0964	307.73	Pos
Cryptochlorogenic acid	0.733941	0.025421	GYFFKZTYAFCTR-AVXPILUSA-N	<chem>C1C(C(C(C(C1(=O)O)O)O)OC(=O)C=CC2=CC(=C(C=C2)O)O)O</chem>	C16H18O9	353.0874	187.845	Neg
D-(+)-Malic acid	0.778794	0.023657	BJEPYKJPYRNKOW-UWTATZPHSA-N	<chem>C(C(C(=O)O)O)C(=O)O</chem>	C4H6O5	133.0143	43.80215	Neg
Benzenepropanamide, N-[2-(acetyloxy)-1-(phenylmethyl)ethyl]-alpha-(benzoylamino)-	0.831489	0.023536	VZPAURMDJZOGHU-UHFFFAOYSA-N	<chem>CC(=O)OCC(CCC1=CC=CC=C1)NC(=O)C(CC2=CC=CC=C2)NC(=O)C3=CC=CC=C3</chem>	C27H28N2O4	445.212	644.515	Pos
(2S,3S,4S,5R,6R)-6-[[[(3S,4R,6aR,6bS,8aS,14bR)-4-(hydroxymethyl)-4,6a,6b,11,11,14b-hexamethyl-8a-[(2S,3R,4S,5S,6R)-3,4,5-trihydroxy-6-(hydroxymethyl)oxan-2-yl]oxycarbonyl-1,2,3,4a,5,6,7,8,9,10,12,12a,14,14a-tetradecahydropicen-3-yl]oxy]-3,4,5-trihydroxyoxane-2-carboxylic acid	0.92628	0.020806	RZQHWSDMLZHIRN-MCTPBCADSA-N	<chem>O=C(O)C1OC(OC2CCC3(C)C4CC=C5C6CC(C)(C)CCC6(C(=O)OC7OC(CO)C(O)C(O)C7O)CCC5(C)C4(C)CCC3C2(C)CO)C(O)C(O)C1O</chem>	C42H66O15	809.4334	503.693	Neg
Quinic acid	0.985566	0.020375	AAWZDTNXLGCEK-LNVDRNJUSA-N	<chem>O=C(O)C1(O)CC(O)C(O)C(O)C1</chem>	C7H12O6	191.0557	169.773	Neg
Citric acid	0.982363	0.018078	KRKNYBCHXYNGOX-UHFFFAOYSA-N	<chem>C(C(=O)O)C(CC(=O)O)(C(=O)O)O</chem>	C6H8O7	191.0197	39.7864	Neg
Ursolic acid	0.848846	0.015258	WCGUUGGRBIKTOS-GPOJBZKASA-N	<chem>O=C(O)C12CCC(C)C(C)C2C3=CCC4C5(C)CCC(O)C(C)(C)C5CCC4(C)C3(C)CC1</chem>	C30H48O3	439.3567	533.181	Pos
9-Hydroxy-10,12,15-octadecatrienoic acid	0.839304	0.015067	RIGGEAZDTKMXSI-UHFFFAOYSA-N	<chem>O=C(O)CCCCCCCC(O)C=CC=CCC=CCC</chem>	C18H30O3	293.2122	705.648	Neg
2-Cyclohexen-1-one, 4-hydroxy-4-(3-hydroxybutyl)-3,5,5-trimethyl-	0.845512	0.013885	CWOFGGNDZOPNFG-UHFFFAOYSA-N	<chem>CC(O)CCC1(O)C(=C(C(=O)CC1(C)C)C</chem>	C13H22O3	209.1537	245.155	Pos
Sinapoyl aldehyde	0.808973	0.013507	CDICDSOGTRCHMG-UHFFFAOYSA-N	<chem>O=CC=CC=1C=C(OC)C(O)=C(OC)C=1</chem>	C11H12O4	209.0806	82.0492	Pos

3,5-Dicaffeoylquinic acid	0.951998	0.012374	KRZBCHWVBQOTNZ-RDJMKVHDSA-N	<chem>C1C(C(C(C(C1(=O)O)O)OC(=O)C=CC2=CC(=C(C=C2)O)O)OC(=O)C=CC3=CC(=C(C=C3)O)O</chem>	C25H24O12	517.1331	346.632	Pos
1,3-Dicaffeoylquinic acid	0.615637	0.011793	YDDUMTOHNYZQPO-UHFFFAOYSA-N	<chem>C1C(C(C(C(C1(=O)O)OC(=O)C=CC2=CC(=C(C=C2)O)O)OC(=O)C=CC3=CC(=C(C=C3)O)O)O</chem>	C25H24O12	515.1202	355.233	Neg
4-Hydroxy-3,5-dimethoxyphenyl 6-O-[(2S,3R,4R)-3,4-dihydroxy-4-(hydroxymethyl)tetrahydro-2-furanyl]-beta-D-glucopyranoside	0.762812	0.011346	BPSJMBKZSUTYNF-GXCUHXBUSA-N	<chem>COC1=CC(=CC(=C1O)OC)O[C@@H]2O[C@H](CO[C@H]3OC[C@](O)(CO)[C@H]3O)[C@@H](O)[C@H](O)[C@H]2O</chem>	C19H28O13	463.1447	132.849	Neg
(1S,4S,5R,10S,13S,17S,19S,20R)-10-hydroxy-4,5,9,9,13,19,20-heptamethyl-24-oxahexacyclo[1.5.5.2.0 <sup>1,18</sup> .0 <sup>4,17</sup> .0 <sup>5,14</sup> .0 <sup>8,13</sup> ]tetracos-15-en-23-one	0.937703	0.01125	UVBLDLGZDSGCSN-MWOWFCOASA-N	<chem>O=C1OC23C=CC4C5(C)CCC(O)C(C)(C)C5CCC4(C)C3(C)CCCC(C)C(C)C26</chem>	C30H46O3	455.3522	610.662	Pos
Ferulaldehyde	0.987928	0.010489	DKZBBWMURDFHNE-NSCUHMNSA-N	<chem>COC1=C(C=CC(=C1)C=CC=O)O</chem>	C10H10O3	179.0701	61.873	Pos

*ADORA2A* (Figure 8A and B). The docking results revealed that ursonic acid had the lowest binding energy with *ADORA2A* (binding energy was  $-4.64$ , Figure 8C).

## NfkbI Was the TF of *ADROA2A*, and Ursonic Acid Might Activate *ADROA2A* Though NFKBI

Immunofluorescence was used to detect *ADORA2A* expression in the *Ilex cornuta* and control groups. The results showed that mice in the *Ilex cornuta* group had more *ADORA2A* expression in the fracture site on days 7 and 14, and the

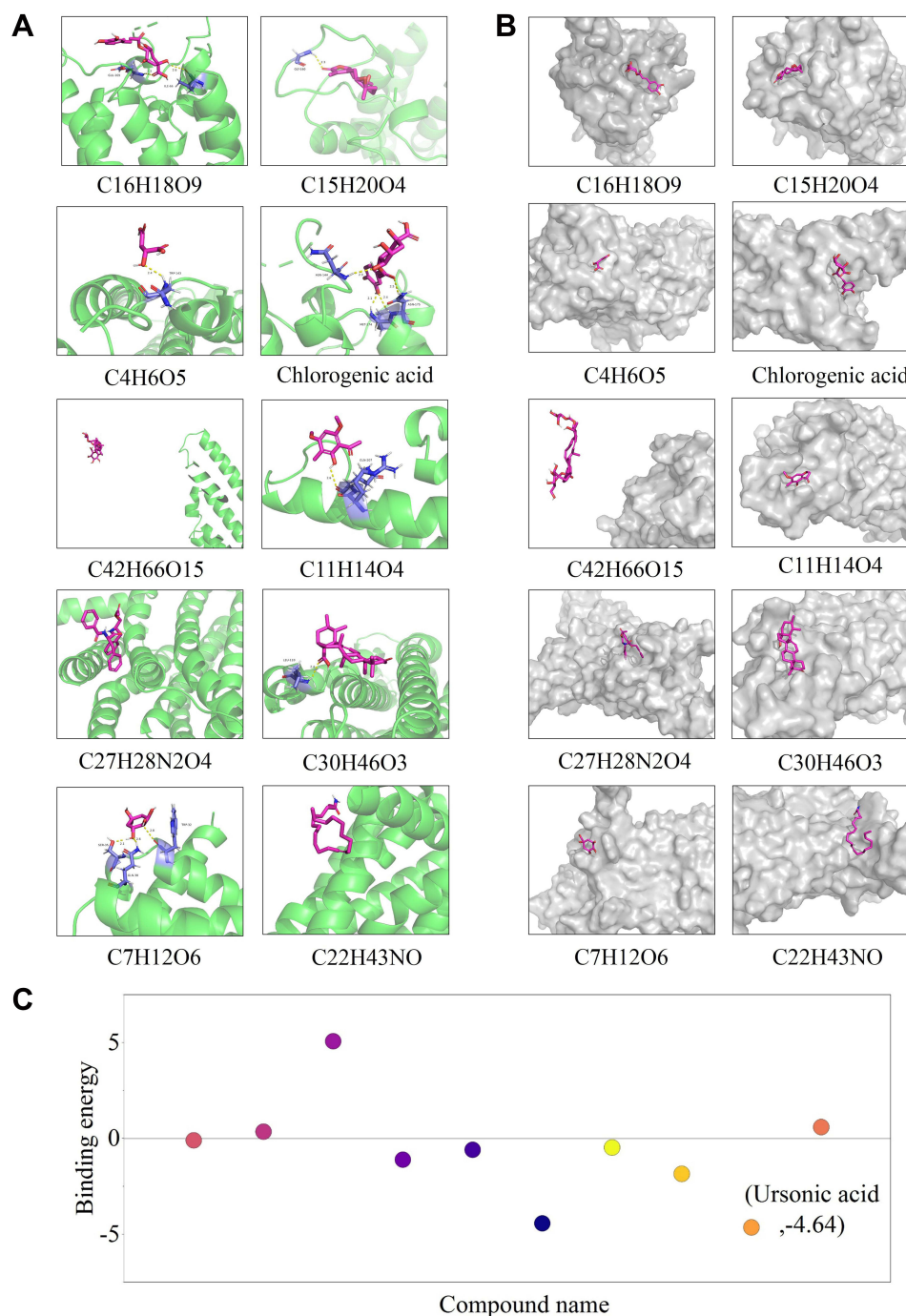


**Figure 8** Molecular docking of the top 10 compounds on *ADORA2A*. (A) The binding condition images. (B) The binding site and the bioactive pocket. (C) The binding energy scatter diagram revealed that ursonic acid had the lowest binding energy with *ADORA2A*.

differences were statistically significant ( $p < 0.05$ ) (Figure 9). To explore the regulatory mechanism of the *Ilex cornuta* bark on *ADORA2A* expression, the TRRUST database and JASPAR 2022 were used to predict the TFs, the binding region of TFs, and *ADORA2A* promoter sequence. Nuclear factor  $\kappa$ B subunit 1 (NFKB1) was the TF of *ADORA2A*, and the binding sequence might be GGGAATTTCC (Figure 10A). Molecular docking methods were used to predict the binding possibility of the compound and NFKB1 (Figure 10B and C). The docking results revealed that ursonic acid had the lowest binding energy with NFKB1 (binding energy was  $-5.28$ , Figure 10D).

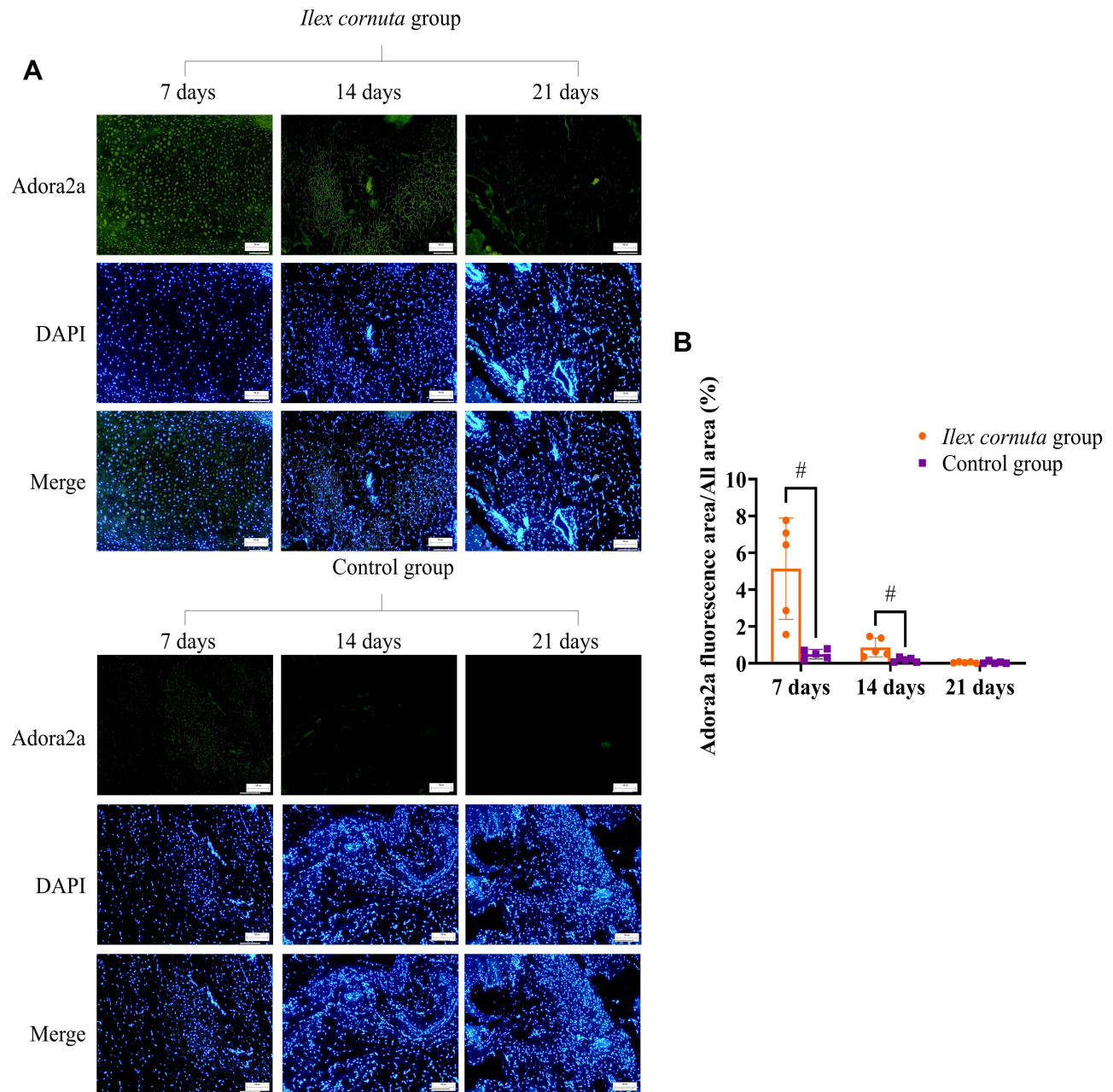


**Figure 9** The Immunofluorescence images of the fracture site. (A) adora2a immunofluorescent staining. *Ilex cornuta* bark treatment promoted adora2a expression at 7,14 days. The contrast and brightness were evenly adjusted for each picture. Immunofluorescent images,  $\times 100$ ; original scale bar,  $50 \mu\text{m}$ . (B) The bar chart revealed the difference between groups, #  $p < 0.05$ .  $n = 5$  at each timepoint.

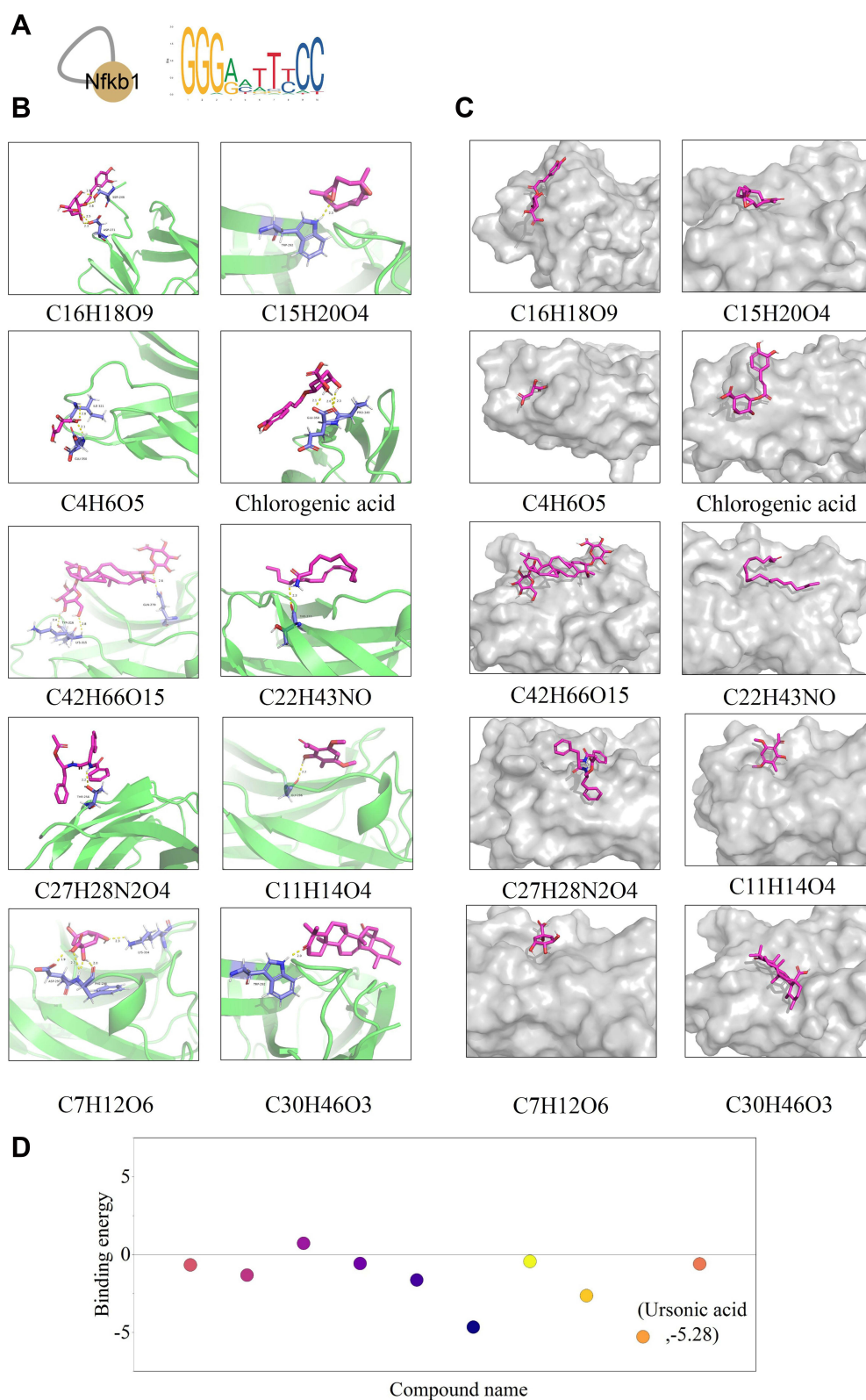


**Figure 10** The TF of adora2a and molecular docking of the top 10 compounds on nfkb1. **(A)** The TRRUST database and JASPAR 2022 showed that nfkb1 was the only one TF of adora2a and the binding sequence might be GGGAATTCC. **(B)** The binding condition images with nfkb1. **(C)** The binding site and the bioactive pocket with nfkb1. **(D)** The binding energy scatter diagram revealed that ursonic acid had the lowest binding energy with nfkb1.



## Discussion

Despite experiencing fracture-related anatomical reduction and rigid fixation, there have still been about 5–10% of patients with bone fracture delayed union and nonunion.<sup>1–4</sup> Therefore, finding methods to promote fracture healing and restore the functional activities of the affected limbs has been an urgent task. Currently, the number of drugs directly accelerating bone healing is limited, especially the extracts directly from plants.

In this study, the effect of the bark of *Ilex cornuta* on bone healing was studied, and the water extraction method was used. Mice received intragastric administration of the water extracts of *Ilex cornuta* bark. The promoting effects of *Ilex cornuta* bark on bone healing were observed by  $\mu$ CT examination as the mice in the *Ilex cornuta* group had more callus. Meanwhile, the biomechanics strength of bone reconstruction was analyzed. *Ilex cornuta* bark treatment could enhance the biomechanics strength of the bone healing process, which could advance the weight-bearing time of the affected limb.

The target genes were clarified by bioinformatics analysis to explore the mechanism of *Ilex cornuta* bark in promoting fracture healing. A total of 206 genes were involved in accelerating bone healing by *Ilex cornuta* bark. The PPI network was used to bring the hub genes to the surface. *ADORA2A* was one of the key genes, and the  $-\log_{10}$ FDR of *ADORA2A* was 4.85389. Additionally, the  $\log_2$ (P-value) of *ADORA2A* was 23.10115. Adora2a is a G-protein coupled receptor, and the adora2a agonist has a promoting tissue healing effect. Mediero et al<sup>7</sup> have put forward that CGS21680 (an adora2a agonist) could enhance bone regeneration as well as BMP-2. Bekisz et al<sup>30</sup> have used the sheep calvarial defect model to discuss the osteogenic capacity of dipyridamole (an adora2a agonist). The results have shown that dipyridamole could significantly improve the calvarial bone regeneration capacity. Witek et al<sup>31</sup> have also proposed that an indirect adora2a agonist enhanced bone formation. Lopez et al<sup>2</sup> have summarized the effect adenosine receptor has on bone healing and found that adora2a activation could accelerate bone healing. Many studies have confirmed the regulating bone healing effects of adora2a.<sup>2,3,8,32</sup>

Immunofluorescence detection of bone fracture site verified the target gene of *Ilex cornuta* bark in bone healing. *Ilex cornuta* bark treatment could boost *ADORA2A* expression in the fracture site on days 7 and 14. The KEGG enrichment analysis was used to explore the involved signal pathways of *Ilex cornuta* bark treatment. Both the cAMP signaling pathway and neuroactive ligand–receptor interaction had 7 enriched genes. *CREB1*, *ADORA2A*, *FSHB*, *ADORA1*, *GNAS*, *FOS*, and *DRD2* were enriched in the cAMP signaling pathway, while *ADORA2A*, *ADORA2B*, *FSHB*, *ADORA3*, *P2RY1*, *ADORA1*, and *DRD2* were enriched in the neuroactive ligand–receptor interaction. The cAMP signaling pathway and neuroactive ligand–receptor interaction were two very important pathways in fracture healing. Many articles have also demonstrated this finding.<sup>33–35</sup>

The non-target metabolomic analysis was used to explore the main compositions of *Ilex cornuta* bark. The results showed 410 main compound compositions of *Ilex cornuta* bark, where 190 were neg ion mode, and 220 were pos ion mode. Molecular docking was used to predict the regulatory effect of the compounds on adora2a, and ursonic acid had the lowest binding energy with adora2a.

Ursonic acid is a naturally existing pentacyclic triterpenoid; however, the pharmacological effects and associated mechanisms of ursonic acid are not well known.<sup>36</sup> Presently, ursonic acid has been demonstrated to have anti-inflammatory and antioxidant effects.<sup>36</sup> Adora2a is also an anti-inflammatory and immune regulatory negative factor. Ursonic acid could bind adora2a to reduce the fracture site excessive inflammatory injury and oxidative stress, which might be the mechanism of *Ilex cornuta* bark in bone healing.

In addition to binding with adora2a, ursonic acid could also regulate *ADORA2A* expression. Nfkb1 is a strong pro-inflammatory factor and can induce cell death. However, it is the only TF of *ADORA2A* in the TRRUST database. Ursonic acid could also bind nfkb1 by molecular docking, which might activate adora2a through Nfkb1. The specific mechanism needs to be confirmed by further research.

The limitations of this study were obvious. As metabolomic analysis showed that *Ilex cornuta* had many compounds in its composition, more studies are needed to clarify that ursonic acid was the effective component in the extract of *Ilex cornuta* bark. Further, *ADORA2A* was up-regulated in the animal by the extract treated, but the target gene was not *ADORA2A* certainly. This also needs to be proved.

## Conclusions

*Ilex cornuta* bark water extract is a plant extract to promote bone healing. Ursonic acid was the most important compound in *Ilex cornuta* bark water extract. Ursonic acid could bind adora2a on the cellular membrane and also Nfkb1 to activate adora2a expression. Adora2a was the key regulator in the bone healing process.

## Data Sharing Statement

The [Supplemental Data](https://data.mendeley.com/datasets/jxbdw4gy32/1) used to support the findings of this study have been deposited in the Mendeley Data repository (data.mendeley.com/datasets/jxbdw4gy32/1).

## Acknowledgments

We thank Beijing Chaoyang hospital and capital medical university for providing the experimental place and the related software used in this study. We thank Wuhan Duobo Technology Co., Ltd for animal sample  $\mu$ CT scanning and Beijing Qinyi Biotechnology Co., Ltd for Non-target metabolomic analysis, Wuhan Servicebio Biotechnology Co., Ltd for Immunofluorescence detection.

## Author Contributions

All authors made a significant contribution to the work reported, whether that is in the conception, study design, execution, acquisition of data, analysis and interpretation, or in all these areas; took part in drafting, revising or critically reviewing the article; gave final approval of the version to be published; have agreed on the journal to which the article has been submitted; and agree to be accountable for all aspects of the work.

## Funding

This research received no specific grant from any funding agency in the public, commercial, or not-for-profit sectors.

## Disclosure

The authors declared no potential conflicts of interest with respect to the research, authorship, and/or publication of this article.

## References

1. Zura R, Xiong Z, Einhorn T, et al. Epidemiology of fracture nonunion in 18 human bones. *JAMA Surg.* 2016;151(11):e162775. doi:10.1001/jamasurg.2016.2775
2. Lopez CD, Bekisz JM, Corciulo C, et al. Local delivery of adenosine receptor agonists to promote bone regeneration and defect healing. *Adv Drug Deliv Rev.* 2019;146:240–247. doi:10.1016/j.addr.2018.06.010
3. Wang D, Wang J, Zhou J, Zheng X. The role of adenosine receptor A2A in the regulation of macrophage exosomes and vascular endothelial cells during bone healing. *J Inflamm Res.* 2021;14:4001–4017. doi:10.2147/JIR.S324232
4. Reahl GB, Gerstenfeld L, Epidemiology KM, Assessments C. Epidemiology, Clinical Assessments, and Current Treatments of Nonunions. *Curr Osteoporos Rep.* 2020;18(3):157–168. doi:10.1007/s11914-020-00575-6
5. Kim J, Kang W, Min H. In vitro anti-inflammatory activity of *Ilex cornuta* extract mediated by inhibition of extracellular signal-regulated kinase phosphorylation. *J Med Food.* 2017;20(10):981–988. doi:10.1089/jmf.2016.3913
6. Yu D, Zhu Z, Wang M, et al. Triterpenoid saponins from *Ilex cornuta* protect H9c2 cardiomyocytes against H<sub>2</sub>O<sub>2</sub>-induced apoptosis by modulating Ezh2 phosphorylation. *J Ethnopharmacol.* 2021;269:113691. doi:10.1016/j.jep.2020.113691
7. Mediero A, Wilder T, Perez-Aso M, Cronstein BN. Direct or indirect stimulation of adenosine A2A receptors enhances bone regeneration as well as bone morphogenetic protein-2. *FASEB J.* 2015;29(4):1577–1590. doi:10.1096/fj.14-265066
8. Zheng X, Wang D. The adenosine A2A receptor agonist accelerates bone healing and adjusts Treg/Th17 cell balance through interleukin 6. *Biomed Res Int.* 2020;2020:2603873. doi:10.1155/2020/2603873
9. Cheng X, Yin C, Deng Y, Li Z. Exogenous adenosine activates A2A adenosine receptor to inhibit RANKL-induced osteoclastogenesis via AP-1 pathway to facilitate bone repair. *Mol Biol Rep.* 2022;49(3):2003–2014. doi:10.1007/s11033-021-07017-1
10. Kim J, Shin JY, Choi YH, et al. Adenosine and cordycepin accelerate tissue remodeling process through adenosine receptor mediated Wnt/ $\beta$ -catenin pathway stimulation by regulating GSK3b activity. *Int J Mol Sci.* 2021;22(11):5571. doi:10.3390/ijms22115571
11. Furuta T, Miyaki S, Ishitobi H, et al. Mesenchymal stem cell-derived exosomes promote fracture healing in a mouse model. *Stem Cells Transl Med.* 2016;5(12):1620–1630. doi:10.5966/sctm.2015-0285
12. Magnusdotir R, Gohin S, Ter Heegde F, et al. Fracture-induced pain-like behaviours in a femoral fracture mouse model. *Osteoporos Int.* 2021;32(11):2347–2359. doi:10.1007/s00198-021-05991-7

13. Shi L, Liu Y, Yang Z, et al. Vasoactive intestinal peptide promotes fracture healing in sympathectomized mice. *Calcif Tissue Int.* 2021;109(1):55–65. doi:10.1007/s00223-021-00820-9
14. Paul GR, Wehrle E, Tourolle DC, Kuhn GA, Müller R. Real-time finite element analysis allows homogenization of tissue scale strains and reduces variance in a mouse defect healing model. *Sci Rep.* 2021;11(1):13511. doi:10.1038/s41598-021-92961-y
15. Johnson D, Lawrence SE, Livingston EW, Hienz RD, Davis CM, Lau AG. Modeling space radiation induced bone changes in rat femurs through finite element analysis. *Annu Int Conf IEEE Eng Med Biol Soc.* 2018;2018:1763–1766. doi:10.1109/EMBC.2018.8512620
16. Fang S, Dong L, Liu L, et al. HERB: a high-throughput experiment- and reference-guided database of traditional Chinese medicine. *Nucleic Acids Res.* 2021;49(D1):D1197–D1206. doi:10.1093/nar/gkaa1063
17. Szklarczyk D, Gable AL, Nastou KC, et al. The STRING database in 2021: customizable protein-protein networks, and functional characterization of user-uploaded gene/measurement sets. *Nucleic Acids Res.* 2021;49(D1):D605–D612. doi:10.1093/nar/gkaa1074
18. Szklarczyk D, Gable AL, Lyon D, et al. STRING v11: protein-protein association networks with increased coverage, supporting functional discovery in genome-wide experimental datasets. *Nucleic Acids Res.* 2019;47(D1):D607–D613. doi:10.1093/nar/gky1131
19. Shannon P, Markiel A, Ozier O, et al. Cytoscape: a software environment for integrated models of biomolecular interaction networks. *Genome Res.* 2003;13(11):2498–2504. doi:10.1101/gr.1239303
20. Otasek D, Morris JH, Bouças J, Pico AR, Demchak B. Cytoscape Automation: empowering workflow-based network analysis. *Genome Biol.* 2019;20(1):185. doi:10.1186/s13059-019-1758-4
21. Tang Y, Li M, Wang J, Pan Y, Wu FX. CytoNCA: a cytoscape plugin for centrality analysis and evaluation of protein interaction networks. *Biosystems.* 2015;127:67–72. doi:10.1016/j.biosystems.2014.11.005
22. Han H, Cho JW, Lee S, et al. TRRUST v2: an expanded reference database of human and mouse transcriptional regulatory interactions. *Nucleic Acids Res.* 2018;46(D1):D380–D386. doi:10.1093/nar/gkx1013
23. Castro-Mondragon JA, Riudavets-Puig R, Rauluseviciute I, et al. JASPAR 2022: the 9th release of the open-access database of transcription factor binding profiles. *Nucleic Acids Res.* 2022;50(D1):D165–D173. doi:10.1093/nar/gkab1113
24. Huang da W, Sherman BT, Lempicki RA. Systematic and integrative analysis of large gene lists using DAVID bioinformatics resources. *Nat Protoc.* 2009;4(1):44–57. doi:10.1038/nprot.2008.211
25. Huang da W, Sherman BT, Lempicki RA. Bioinformatics enrichment tools: paths toward the comprehensive functional analysis of large gene lists. *Nucleic Acids Res.* 2009;37(1):1–13. doi:10.1093/nar/gkn923
26. Berman HM, Westbrook J, Feng Z, et al. The protein data bank. *Nucleic Acids Res.* 2000;28(1):235–242. doi:10.1093/nar/28.1.235
27. Burley SK, Bhikadiya C, Bi C, et al. RCSB Protein Data Bank: celebrating 50 years of the PDB with new tools for understanding and visualizing biological macromolecules in 3D. *Protein Sci.* 2022;31(1):187–208. doi:10.1002/pro.4213
28. Little JL, Williams AJ, Pshenichnov A, Tkachenko V. Identification of “known unknowns” utilizing accurate mass data and ChemSpider. *J Am Soc Mass Spectrom.* 2012;23(1):179–185. doi:10.1007/s13361-011-0265-y
29. Seeliger D, de Groot BL. Ligand docking and binding site analysis with PyMOL and Autodock/Vina. *J Comput Aided Mol Des.* 2010;24(5):417–422. doi:10.1007/s10822-010-9352-6
30. Bekisz JM, Flores RL, Witek L, et al. Dipyridamole enhances osteogenesis of three-dimensionally printed bioactive ceramic scaffolds in calvarial defects. *J Craniomaxillofac Surg.* 2018;46(2):237–244. doi:10.1016/j.jcms.2017.11.011
31. Witek L, Alifarag AM, Tovar N, et al. Repair of critical-sized long bone defects using dipyridamole-augmented 3D-printed bioactive ceramic scaffolds. *J Orthop Res.* 2019;37(12):2499–2507. doi:10.1002/jor.24424
32. Wang D, Wang J, Zheng X. Genes and pathways of regulatory T cells regulated by adenosine A2A receptor: a bioinformatics study. *All Life.* 2021;14:1043–1053. doi:10.1080/26895293.2021.1999861
33. Zhou W, Yu L, Fan J, et al. Endogenous parathyroid hormone promotes fracture healing by increasing expression of BMP2 through cAMP/PKA/CREB pathway in mice. *Cell Physiol Biochem.* 2017;42(2):551–563. doi:10.1159/000477605
34. Khan K, Pal S, Yadav M, et al. Prunetin signals via G-protein-coupled receptor, GPR30(GPER1): stimulation of adenylyl cyclase and cAMP-mediated activation of MAPK signaling induces Runx2 expression in osteoblasts to promote bone regeneration. *J Nutr Biochem.* 2015;26(12):1491–1501. doi:10.1016/j.jnutbio.2015.07.021
35. Jiang X, Chen W, Shen F, et al. Pinoresinol promotes MC3T3-E1 cell proliferation and differentiation via the cyclic AMP/protein kinase A signaling pathway. *Mol Med Rep.* 2019;20(3):2143–2150. doi:10.3892/mmr.2019.10468
36. Son J, Lee SY. Therapeutic potential of ursolic acid: comparison with ursolic acid. *Biomolecules.* 2020;10(11):1505. doi:10.3390/biom10111505

## Drug Design, Development and Therapy

Dovepress

### Publish your work in this journal

Drug Design, Development and Therapy is an international, peer-reviewed open-access journal that spans the spectrum of drug design and development through to clinical applications. Clinical outcomes, patient safety, and programs for the development and effective, safe, and sustained use of medicines are a feature of the journal, which has also been accepted for indexing on PubMed Central. The manuscript management system is completely online and includes a very quick and fair peer-review system, which is all easy to use. Visit <http://www.dovepress.com/testimonials.php> to read real quotes from published authors.

Submit your manuscript here: <https://www.dovepress.com/drug-design-development-and-therapy-journal>